Journal of Applied Fluid Mechanics, Vol. 14, No. 4, pp. 1249-1255, 2021.
Available online at www.jafmonline.net, ISSN 1735-3572, EISSN 1735-3645.
https://doi.org/10.47176/jafm.14.04.32464

Flow Conditions Influence on the Instability of a Pump Characteristic

A. Lipej

University of Novo mesto Faculty of Mechanical Engineering, Novo mesto, 8000, Slovenia

†*Corresponding Author Email: andrej.lipej@fs-unm.si*

(Received December 13, 2020; accepted January 28, 2021)

ABSTRACT

The operating range of centrifugal pumps is a very important information for the long service life and risks regarding various premature failures. The pump cannot always operate within the permitted range, for example, it must start and shut down the operation. When developing and selecting a pump, it is necessary to take into account the fact that the pump should be operated close to the best efficiency point (BEP) as often as possible. In this paper, we discuss the kinematic causes for the formation of the so-called hump zone in the pump H(Q) characteristic, where the flow rates are smaller than at the BEP. For the case of a reversible pump turbine, the detailed course of the pump characteristic at different relative openings of the guide vanes was numerically analyzed. The article presents the detailed flow field of velocity vectors and streamlines in front of the runner, inside the runner, and behind the runner.

Keywords: Centrifugal pump; Operation characteristics; Computational fluid dynamics.

NOMENCLATURE

H	head	U	velocity
H_{BEP}	head in best efficiency point	v	velocity
k	turbulence kinetic energy	x	length from center of cone
L	length scale	y^+	non dimensional
n	rotational speed	ζ_i	constant
P_k	turbulence production term	κ	von Karman constant
Q	flow rate	μ_t	eddy viscosity
Q_{BEP}	flow rate in best efficiency point	ρ	density
S_{ij}	strain rate tensor	σ_k	constant
t	time		

1. INTRODUCTION

The centrifugal pump impeller is always designed so that the geometric angles of the blades match the angles of the velocity vectors when the pump is operating near BEP. When the pump is operating at part load or at flows higher than BEP, the angles of the velocity vectors at the inlet and outlet modify and this change affects certain operating disturbances, the formation of areas of flow separation and recirculation.

Normally, the pump can operate permanent in the range between 0,7 and 1,2 Q/Q_{BEP}. For smaller specific speeds, this range is slightly larger, but for larger ones it narrows. In addition to unstable operating characteristics in part load, there is also a risk of pressure pulsations, vibrations, cavitation (Leonard 2015, Limbach *et al*. 2016) and an increase in the axial thrust (Florjančič 2008).

In the literature it is possible to find a lot of studies which deal with pump characteristics. A detailed presentation of numerical methods about the flow analysis in reversible pump-turbines can be found in the dissertation (Ješe 2015). Also research that is more focused on experimental methods shows us a detailed course of the characteristics of pumps in the entire operating range (Yang *et al*. 2015). Some papers are more focused in a study of the influence of individual parts of the machine (Jia *et al*. 2019).

However, very few studies have been published that analyze in detail the causes of all possible problems in the operation of centrifugal pumps. This is important mainly due to the fact that well-known causes help us to reduce or eliminate problems.

In the case of reversible pump turbines, instability in operation occurs at certain flows that are lower than the optimum, which is reflected in the H(Q) characteristic. The normal H(Q) characteristic decreases with increasing flow. In this case, however, we obtain at partial flows the so-called hump zone, which may be more or less pronounced.

In some cases, this area is barely noticeable in the characteristics, and in some cases it is very well developed.

In this paper, we discussed two different pumps with different specific rotational speeds. Reversible pump turbines also differ in the shape of the cone in front of runner.

In the analysis of flow conditions, we focused on four segments. The first part is the area at the exit of the draft tube in the cone or the area in front of the runner.

The second part represents the region of flow conditions in the inter blade space of the runner. The third part represents the flow conditions between the stator blades and the fourth part the flow in the spiral casing.

If we analyze the flow conditions near the optimal operating point, the flow in most parts of the machine is such that it follows the hydraulic shape of individual parts. In stationary parts absolute flow is analyzed and in rotating parts relative flow is analyzed. In most cases, no vortices, flow separation, or backflows are observed.

When the operating mode starts to move to the left direction according to the characteristic, or when the flows decrease, recirculation starts to appear at the entrance to the runner. Cone recirculation changes the flow conditions at the input to the runner and also has a strong effect on the flow conditions inside (Lipej and Mitruševski 2016).

Recirculation can be the cause of the cavitation, which according to the NPSH characteristic in the pump should not be present. This is a special influence of recirculation on the formation of cavitation, which occurs in operating areas that are supposed to be safe from cavitation if we consider the NPSH characteristic.

An interesting consequence of such cavitation is also the area where cavitation occurs. The consequences can be noticeable on the pressure side of the rotor blades, where under normal conditions the pressure is high enough to prevent cavitation.

We found that in some cases the occurrence of recirculation is already associated with the formation of a hump zone in the characteristic, and in some cases we observe instability in the characteristic even before the occurrence of recirculation. In both observed cases, we performed a more detailed analysis of the velocity field at the runner input.

In particular, we analyzed the distribution of the axial velocity component as a function of radius in several places.

2. NUMERICAL METHOD

In this paper, we discussed two reversible pump turbines in pump mode with specific speed n_q=42 and n_q=60.

$$n_q = n\frac{Q^{\frac{1}{2}}}{H^{\frac{3}{4}}} \tag{1}$$

For a pump with a higher specific speed, the paper presents numerical and experimental results. For a pump with a lower specific speed, only numerical results of individual characteristics and detailed results of current conditions in the entire considered domain are presented. For a pump with a lower specific speed, we analyzed two different geometries, where we changed the inlet and outlet angles of the runner.

Figure 1 shows the geometry of both analyzed runners in the paper. Both runners were calculated at model size.

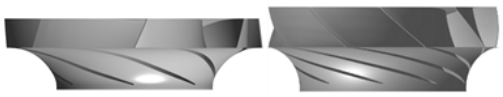

Fig. 1. Geometry of both analyzed runners – left n_q=42, right n_q=60.

We wanted to show how the range of instability at the H(Q) characteristic can be predicted fairly accurately using CFD. Therefore, we performed several numerical analyses of the pump characteristics and compared the results with the measurement results on the model. The complete computational domain, which contains draft tube with extension, runner, guide vanes, stay vanes and spiral casing, is presented in Fig. 2.

Fig. 2. Computational domain.

We also wanted to analyze the kinematics of the flow in the individual parts of the pump in order to determine the main flow characteristics that influence the formation of an unstable area in the characteristic.

The first prerequisite for accurate numerical analysis is a quality numerical grids (Fig. 3). In areas where we wanted a really accurate result, we created structured computational grids that meet all the criteria regarding orthogonality, expansion ratio and aspect ratio.

The computational grids in draft tube and in the

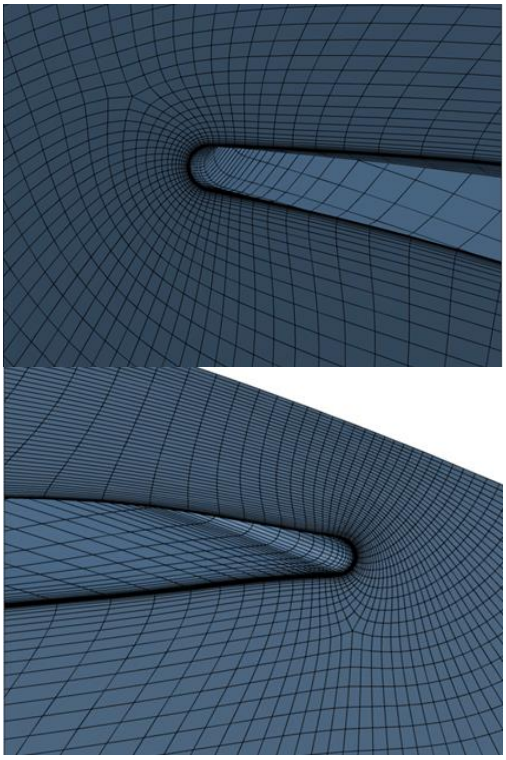

Fig. 3. Computational grid around leading and trailing edge of impeller blade.

spiral casing are unstructured. Complete computational grids consist of around fifteen millions of elements. The quality of all computational grids was satisfied with recommended parameters obtained by experience from many previous successful finished projects.

The dimensionless parameter y^+ was ensured to be less than 5 at the majority of surfaces in all parts. The distribution of the y^+ parameter on the runner walls is shown in Fig. 4.

Due to the calculation of the flow conditions at different flow rates, y^+ cannot be the same for all operating modes, but the differences are small enough that they do not significantly affect the results of the numerical analysis.

Numerical analysis was done using different turbulence models. Because in most industrial applications it is not possible to model turbulence by the direct numerical method, different turbulence models are used.

These cannot resolve all orders of magnitude of turbulence fluctuations. Most models are based on so-called Reynolds average Navier-Stokes equations (RANS). Models can be based on eddy-viscosity or Reynolds stress models.

Particular attention should be paid to the appropriate use of turbulence models when we have the presence of vortices, backflows, and current detachment in the flow.

For the above-mentioned cases and when we want to analyze the flow conditions in the boundary layer in detail, the turbulent model k-ω SST is recommended. That is why for steady state analysis k-ω SST turbulence model was used.

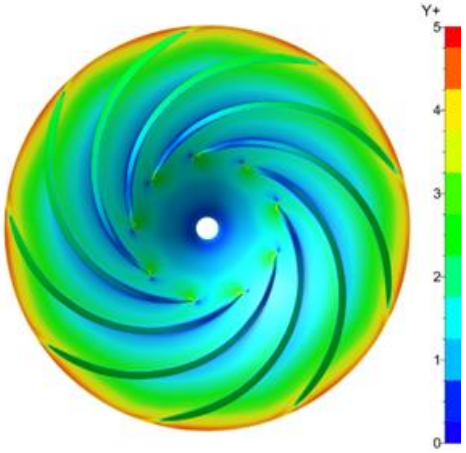

Fig. 4. Distribution of non-dimensional parameter y^+ in the impeller.

For cases where the flow conditions change over time, nonstationary turbulence models should be used. In such cases, Unsteady Reynolds Averaged Navier-Stokes (URANS) models can be used, but these models are also not able to model accurately all orders of magnitude of turbulent fluctuations.

For the cases discussed in this paper, enhanced turbulent models called Scalable Adaptive Simulation (SAS) Shear Stress Transport (SST) can be used. With them it is possible to solve different orders of magnitude of turbulent structures. Various turbulent structures in SAS models are resolved by introducing the von Karman length scale.

The SAS models are similar to LES (Large Eddy Simulation) turbulence models in areas where the flow conditions are predominantly non-stationary, but in more stable zones it works similarly to RANS models.

The SAS model (Menter 2015) is defined as a two-equation turbulence model, with the variable $\Phi=\sqrt{k}L$ for the scale equation:

$$\frac{\partial(\rho k)}{\partial t}+\frac{\partial\left(\rho\bar{U}_j k\right)}{\partial x_j}=P_k-c_\mu^{\frac{3}{4}}\rho\frac{k}{\Phi^2}+\frac{\partial}{\partial x_j}\left(\frac{\mu_t}{\sigma_k}\frac{\partial k}{\partial x_j}\right) \tag{2}$$

$$\frac{\partial(\rho\Phi)}{\partial t}+\frac{\partial\left(\rho\bar{U}_j\Phi\right)}{\partial x_j}=\frac{\Phi}{k}P_k\left(\zeta_1-\zeta_2\left(\frac{L_t}{L_{vK}}\right)^2\right)-\zeta_3\rho k+\frac{\partial}{\partial x_j}\left(\frac{\mu_t}{\sigma_\Phi}\frac{\partial\Phi}{\partial x_j}\right) \tag{3}$$

$$\mu_t=c_\mu^{\frac{1}{4}}\rho\Phi \tag{4}$$

The most important new term of scale adaptive model in comparison with standard RANS model is the von Karman length:

$$L_{vK} = \kappa \left| \frac{\bar{U}'}{\bar{U}''} \right| \tag{5}$$

$$\bar{U}' = S = \sqrt{2 S_{ij} S_{ij}}; \bar{U}'' = \sqrt{\frac{\partial^2 \bar{U}_i}{\partial x_j \partial x_j} \frac{\partial^2 \bar{U}_i}{\partial x_k \partial x_k}}$$

$$S_{ij} = \frac{1}{2}\left(\frac{\partial \bar{U}_i}{\partial x_j} + \frac{\partial \bar{U}_j}{\partial x_i} \right) \tag{6}$$

Because of all above mentioned advantages for unsteady calculations we used in our research of pumps characteristics unsteadiness the so called scale resolving SAS-SST turbulence model.

3. NUMERICAL AND EXPERIMENTAL RESULTS

3.1 Analysis of pump - n_q=60

For both pumps we performed the extensive numerical analyses of complete H(Q) and efficiency characteristics and for the first pump also the complete model measurements which enable us to validate the accuracy of numerical results.

Model test was performed on the test rig with high accuracy and repeatability utilizing the latest measuring instruments in accordance with all the requirements, specified in the IEC 60193 standard (IEC (1999). The model diameter of the runner is generally between 0.3 m and 0.35 m. The maximum possible flow rate on the model is 6500 m^3/h and the maximum possible head is 82m.

The first calculation was done using steady state analysis.

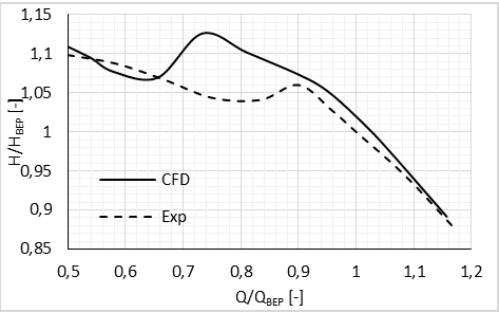

Fig. 5. Numerical and experimental results of steady state analysis – *H(Q)* characteristic.

A comparison of these results is shown in Fig. 3, where it is observed that the onset of the unstable operation range is significantly shifted towards smaller flows and therefore the results are not the best.

We can also see in the Fig. 5 that the matching of the numerical and experimental results is fairly good outside the unstable operating range, although we know that the flow conditions are very non-stationary, especially at wide range of part load.

Calculations were repeated for the same boundary conditions using a nonstationary model. The length of time step was equal to 4° with respect to rotating angle of the runner.

We decided on such a value on the basis of previous results in similar analyses. A comparison of the results numerical and experimental results shows a fairly good numerical prediction of the onset of instability.

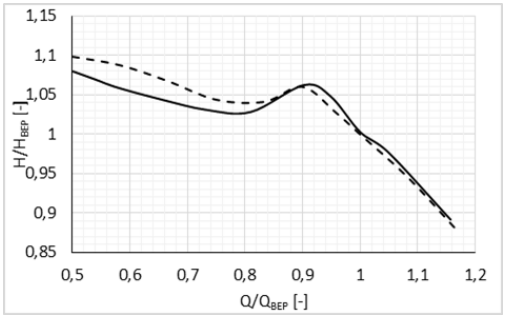

Fig. 6. Numerical and experimental results of unsteady analysis – *H(Q)* characteristic.

The dH/dQ gradient also matches well (Fig. 6), as can be seen from the slope of the increasing part of the H(Q) curve. The agreement in the area of lower flow rates is slightly worse, because obviously even with a nonstationary model we do not list well all nonstationary phenomena in the flow itself.

For non-stationary conditions, we also made a comparison of the efficiency in a wide flow range from 0.5 Q/Q_{opt} to almost 1.2 Q/Q_{opt}. In this case, however, the situation is exactly the opposite as with the H (Q) characteristic, as the match of numerical and experimental results is quite good in the range on the left of the optimum, and the match is worse at flow rates higher than the optimal operating regime (Fig. 7).

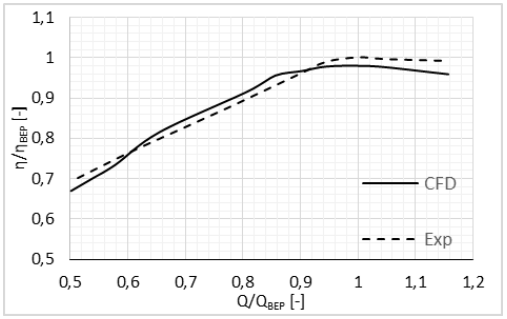

Fig. 7. Numerical and experimental results of unsteady analysis – efficiency.

3.2 Analysis of pump - n_q=42

All items in the title block should be centered across In order to better understand the causes of the formation of the unstable zone in the H(Q) characteristic, we analyzed the flow conditions in the area in front of the impeller in detail.

In the cone of the draft tube, 2D flow were presented on a vertical cross section to identify

possible irregularities in the flow conditions in front of the impeller. Figure 8 presents the results for four operating points from the lowest flows to the optimal operating mode.

At the lowest flow rates, a large area of back flow is observed on both sides of the cone. The vortex region, depending on the increase in flow, moves up the cone and disappears near the optimal operating condition.

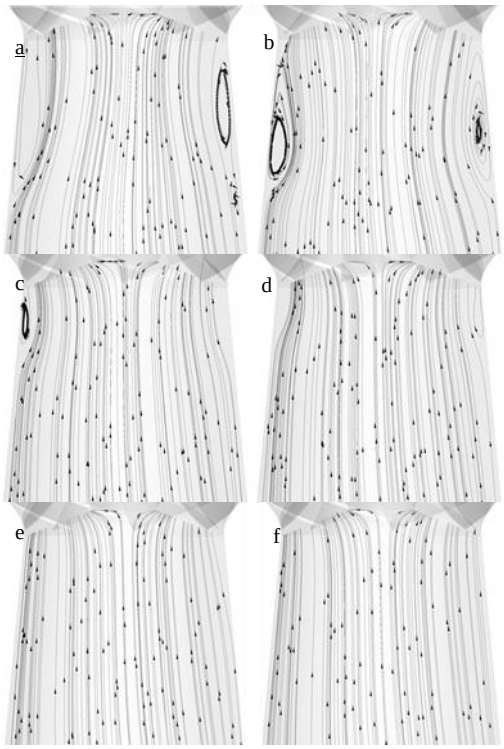

Fig. 8. Recirculation zone in front of impeller for different operating regimes – a) Q/Q_{opt} = 0,61, b) Q/Q_{opt} = 0,70, c) Q/Q_{opt} = 0,73, d) Q/Q_{opt} = 0,77, e) Q/Q_{opt} = 0,81, f) Q/Q_{opt} = 0,96.

The formation and disappearance of the vortex occurs in the region of the unstable characteristic, so that by analyzing the input vortex to some extent of accuracy we can predict the approximate location of the instability in the H(Q) characteristic.

Since the draft tube has an elbow shape, we cannot speak of a completely axisymmetric flow in the cone of the draft tube. If we analyze the flow conditions at another cross-section, the picture would be partially changed, but the global picture regarding the size of the back flow and vortex range would not change.

In addition to 2D stream lines, we also analyzed in detail the distribution of the axial velocity component at the two cross sections in front of the impeller.

The results are shown in Figs. 9 and 10. The cross section, which was distant from the runner inlet 30 mm, clearly shows the impact of the hub and a fairly large area where the axial velocity has negative values.

On the axial velocity graph, we can see that at lower flows, the largest negative values are located further away from the impeller, as already shown in Fig. 10.

At a cross section further away from the runner, the negative axial velocity range is smaller. However, a smaller range of negative velocities can still be observed at the lowest flows.

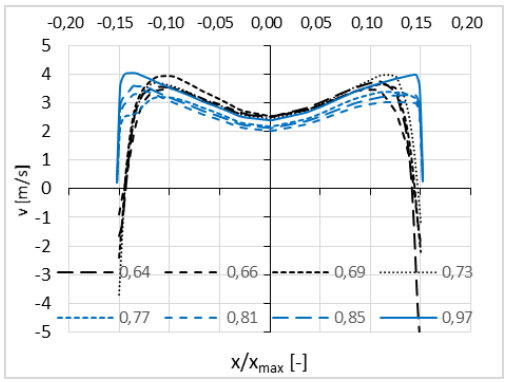

Fig. 9. Axial velocity distribution in front of impeller – first cross section.

If we analyze the flow conditions downstream in detail, we observe similar flow irregularities in the same operating regimes. In operating conditions, where a backflow has occurred in front of the rotor, well-developed vortices can also be observed in the space between impeller blades.

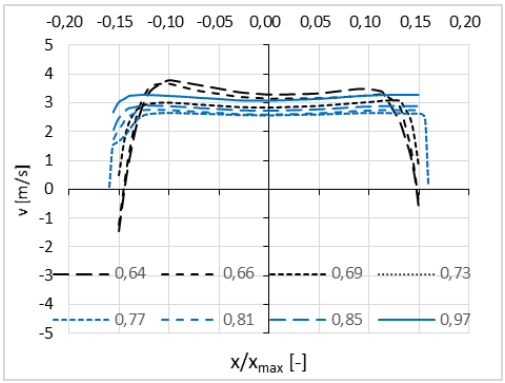

Fig. 10. Axial velocity distribution in front of impeller – second cross section.

Such an example is presented in Fig. 11. The flow conditions between the individual channels of the impeller blades are not the same, which is due to the non-stationary flow conditions and the uneven distribution of speed at the entrance to the runner.

If we analyze the flow conditions in the impeller outside the area of instability of the characteristic H(Q), we see a very nice flow field in the whole impeller (Fig.12).

Fig. 11. Flow inside the impeller Q/Q_{opt} = 0,73 – hump zone.

Fig. 12. Flow inside the impeller Q/Q_{opt}= 0,96 – outside hump zone.

Furthermore, irregularities in the flow conditions are also observed between the stator blades and, last but not least, in the spiral casing. In the area of the unstable characteristic, Fig. 13 shows a strong vortex flow field in vertical section through a spiral casing. This is especially pronounced on the left side of the image, where there is a round cross section with a smaller diameter.

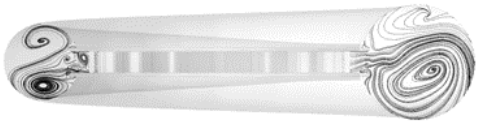

Fig. 13. Flow inside the spiral casing Q/Q_{opt}= 0,73 – hump zone.

The flow conditions in the vicinity of the optimal operating regime show a fairly orderly flow in the stator cascade and also on both sides of the spiral casing (Fig. 14).

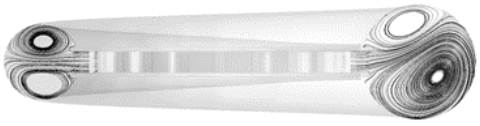

Fig. 14. Flow inside the spiral casing Q/Q_{opt}= 0,96 – near BEP

Based on the presented results for the impeller R1, we designed a new impeller R2 for the same operating conditions. With small changes in the inlet and outlet angles of the rotor blades and slightly changed profile lengths, we obtained a new geometry with a reduced area of instability in the H(Q) characteristic.

Figure 15 shows the H(Q) characteristic for both geometries and we can observe that at higher flows the characteristics are almost completely matched, and at lower flows a reduced range of instability is noticed. The results in Figs, 15 and 16 are obtained by unsteady calculations.

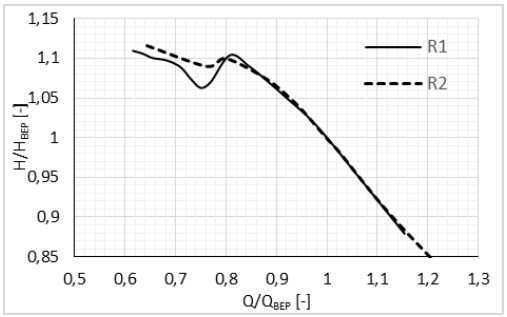

Fig. 15. Comparison of pump characteristics for initial (R1) and optimized final (R2) design.

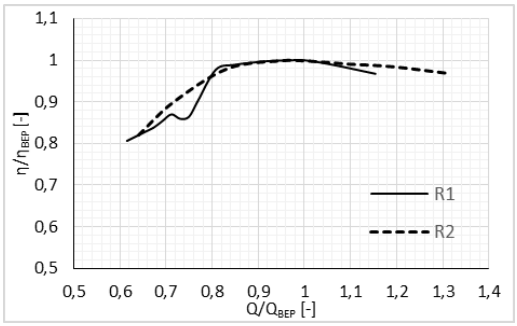

Fig. 16. Comparison of pump efficiency for initial (R1) and optimized final (R2) design.

Small changes are also observed in the efficiency characteristic (Fig. 16), which are noticeable on both sides of the characteristic. Near the optimal operating point, both characteristics match very well. The largest difference is observed in the hump zone, where the largest difference is also in the characteristic H(Q).

Changes are also observed in the analysis of the flow conditions in individual parts of the pump, as there are no such pronounced areas of return flow, detachment and vortices.

5. CONCLUSION

Pump's characteristics can have very different shapes. Therefore, we decided to analyze in a more detailed how the flow conditions affect the instabilities in the pumping characteristics. We analyzed several impellers in detail.

In the first case, we performed a comparison of the results obtained with numerical analyzes and model measurements.

We found that the hump zone can be well analyzed only using nonstationary methods.

A comparison of the latter showed that with numerical analyzes we can predict irregularities in the characteristics quite well. Computation times are actually much longer, but due to the quality of the results, such a procedure is necessary.

In the second case, we presented the development of a new impeller. At the beginning we analyzed the first impeller in development phase, where we already got fairly good desired characteristics, only the hump zone area was slightly over-emphasized.

Based on the initial numerical results, we corrected the design in a few iterations and with repeated numerical analyzes found an improvement in the characteristic in the hump zone.

With obtained results of the presented research, we can conclude that using quality computational grids, suitable numerical methods and turbulent models, it is possible to successfully design new hydraulic shapes of pumps with characteristics that allow long life and minimal maintenance costs.

REFERENCES

Florjančič, D. (2008). *Trouble-Shooting Handbook for Centrifugal Pumps*. Turboinštitut d.d.

IEC 60193 (1999-11). Hydraulic turbines, storage pumps and pump-turbines - Model acceptancetests, ISBN: 2-8318-4993-4 – ICS code: 27.140 – TC 4 – 569.

Ješe, U. (2015). *Numerical Study of Pump-Turbine Instabilities : Pumping Mode off - Design Conditions.* Doctoral thesis, L'Universite Grenoble Alpes, pp. 135.

Jia, J., J. F. Zhang, Y. J. Qu, H. K. Cai, and S. B. Chen. (2019). Study on Hump Characteristics of Pump Turbine with Different Guide Vane Exit Angles. IOP Conference Series: Earth and Environmental Science 240 072038.

Leonard, D. J. (2015). *Computation and Analysis of Cavitating Flow in Francis-Class Hydraulic Turbines*. The Pennsylvania State University.

Lipej, A. and D. Mitruševski (2016). Numerical Prediction of Inlet Recirculation in Pumps. *International Journal of Fluid Machinery and Systems* 9(3). 277–86.

Limbach, P., T. Müller, M. Blume and R. Skoda (2016). Numerical and Experimental Investigation of the Cavitating Flow in a Low Specific Speed Centrifugal Pump and Assessment of the Influence of Surface Roughness on Head Prediction. In *International Symposium on Transport Phenomena and Dynamics of Rotating Machinery*. pp. 1–9

Menter, F. R. (2015). *Best Practice : Scale - Resolving Simulations in ANSYS CFD*. (November 2015).

Yang, J., G. Pavesi, G. Cavazzini and G. Ardizzon (2015). Experimental Characterization of a Pump – Turbine in Pump Mode at Hump Instability Region. *Journal of Fluids Engineering, ASME* Vol. 137 (5).